The Effects of Surface Defects on the Fatigue of Water and Oil Lubricated Contacts

N. Gao and R. S. Dwyer-Joyce

Department of Mechanical Engineering

University of Sheffield, Mappin Street, S1 3JD, UK

Abstract

A study into effects of surface defects on rolling contact fatigue of brass and rail steel has been undertaken on a twin-disc rolling-sliding test machine with both oil and water lubrication. Furrows and dents were artificially introduced into the disc surfaces, and surface micro cracks and pits were monitored by means of surface replication. The results showed that artificial dents only reduce the fatigue life of the contact with oil, but not water lubrication. With oil lubrication the fatigue failure initiates at the surface defect. However with water as a lubricant the whole of the surface undergoes cracking with the defect having no preferential effect. The possible mechanisms behind this behaviour are discussed in this paper.

Keywords: surface defect, fatigue, lubricated contact

NOTATION

a	radius of semi-circular crack
c	half width of Hertzian contact
E^*	reduced elastic modulus
$Ft\,\mathrm{max}$	dimensionless shear stress intensity factor
G	dimensionless material parameter
$h_{\min}$	minimum film thickness
H	hardness
$H_{\min}$	dimensionless minimum film thickness
Ks	tensile stress intensity factor
$Ks\,\mathrm{max}$	maximum tensile stress intensity factor
$Ks\,th$	threshold tensile stress intensity factor
Kt	shear stress intensity factor
$Kt\,\mathrm{max}$	maximum shear stress intensity factor
$Kt\,th$	threshold shear stress intensity factor
L	width of line contact

p	normal surface stress
p_0	maximum Hertzian surface stress
q	tangential surface stress
R	reduced radius of curvature
u_1, u_2	test and conterface disc surface speed
U	dimensionless speed parameter
$\bar{U}$	average entrainment velocity
W	dimensionless load parameter
$\bar{W}$	applied load
a	pressure viscosity coefficient
b	arrow headed crack spread angle
h_0	viscosity at ambient pressure
m	coefficient of surface traction
Λ	film thickness parameter
s_1, s_2	RMS surface roughness of test and conterface disc

1. INTRODUCTION

It is well known that rolling contact fatigue affects the performance of many kinds of machine element, including gears, rolling-element bearings, rolls in the steel-making process, railway wheels and rails. Since Way's pioneering work [1], numerous investigations have been conducted from different points of view. The introduction of powerful computers and advanced solution methods has enabled sophisticated theoretical study of rolling contact fatigue life [2]. However, the mechanism of failure is complex and a conclusive theory is yet to be established. Many factors have to be considered, such as contact stress [3, 4], elastohydrodynamic oil-film thickness [5, 6] residual stress [7, 8], surface traction [9], and their mutual interactions.

Surface roughness and the presence of surface defects is also known to be an important factor [10, 11]. The as manufactured roughness affects fatigue life; in addition, surface damage may be caused during element manufacture, handling or during running. The presence of a dent or scratch will change the contact conditions and may result in a significant reduction in the life of the component. Contact stress distributions are modified by the presence of an indentation resulting in a stress concentration. Surface dents have been shown to modify significantly the formation of elastohydrodynamic lubricant films between rolling elements [12-14]. Several workers [11, 15, 16] have created artificial defects on contact surfaces and studied the effect these have on contact fatigue. Most studies are based on observation and analysis of failed specimens. It is harder to obtain continuous observation of crack initiation and propagation [17, 18]. This often results in some disagreement over the mechanism of contact fatigue failure. In addition, many papers have been published on the subject of rolling contact fatigue,

either under oil or water lubrication, whilst few compare the fatigue effects of surface defects with either oil or water lubrication.

This work has, in part, been motivated by the study of the effects of surface defects on railway track. The wheel/rail interface may undergo water (i.e. rain) contamination or deliberate lubrication by the application of mineral oils or greases to reduce track wear. In an early paper [19] the current authors used a continuous replication process to study initiation and crack growth at various size and shape dents on the surface of oil lubricated brass. In this study, the work has been extended to include rail steel under a range of pressures and with both water and oil lubrication.

2. EXPERIMENTAL PROCEDURE

2.1. Test machine

The rolling contact fatigue experiments were conducted in the laboratory using a twin-disc rolling-sliding test machine. The discs are loaded together hydraulically and driven by two independent electric motors. A computerised control system accurately achieves a desired slide-roll ratio[1], and monitors driving torque. Lubricants are applied using a gravity drip fed system so as to maintain a constant meniscus of liquid in the inlet region. Further details of this test apparatus may be found in reference [20].

2.2. Materials and specimens

The materials tested were a 60/40 brass with an $a + b$ microstructure, a pearlitic rail steel, and a mixed pearlitic and ferritic wheel steel. The chemical composition and mechanical properties of disc materials are given in Table 1. Rail and wheel test discs were cut from wheel rims and rail sections. The wheel discs act as drivers whilst the rail discs are driven (follower discs). All cutting and machining operations were conducted to maintain the original microstructure and properties. Discs were machined to the dimensions of 47 mm in diameter and 10 mm in width [19]. The running surface of each disc was ground to an average roughness of $R_a = 0.35\ \textbf{\textit{m}}m$. The dimensional tolerance of the discs was measured for roundness and eccentricity using a Talyrond profilometer.

Four types of defect were manufactured on the follower disc; transverse or longitudinal scratches, and conical or pyramidal dents. The width and length of the furrows were approximately 0.1-0.3 mm and 5 mm respectively. They were made on a lathe by a cutting tool with a carbide tip (with a tip radius of about 0.05 mm). The conical and pyramidal dents of 0.4-1.2 mm in diameters were made by using a Rockwell and a Vickers testing machine with different loads.

---

[1] Slide-roll ratio is defined here as $200(u_1 - u_2)/(u_1 + u_2)$. $u_1 =$ test disk surface speed; $u_2 =$ counterface disk surface speed. The negative slide-roll ratio implies the test disk is slower than the counterface (i.e. it is the driven disk).

2.3. Test procedure

Rolling contact tests were conducted under a maximum contact pressure of either 600 or 750 MPa for brass, and 900 or 1500 MPa for rail and wheel steels. These represent typical loads experienced in wheel/rail contacts. For the brass tests the aim was to maintain a comparable ratio of p_0/H (peak contact pressure divided by hardness). The slide-roll ratio was set to -1%. The contact area was lubricated using a gravity drip system supplying approximately 1 drip per second for water, or 1 drip per 3 second for oil. Test conditions are shown in Table 2.

A computer-controlled non-contact eddy current crack detection unit was used to monitor the full width of the disc during the tests. In this study failure was defined as the number of rolling cycles required to achieve a crack deep enough to trigger a pre-set alarm level on the eddy current flow detection unit. A critical depth of 400-500 mm was chosen on the basis of previous work [20-22] on the detectability of cracks. Tests were regularly interrupted to take replicas of the disc surface, and record the weight and disc dimensions. Selected disks were sectioned and the crack morphology studied using an optical microscope and a scanning electron microscope (SEM). The microhardness variation with depth below the contact surface was also measured.

3. EXPERIMENTAL RESULTS

3.1 Coefficient of traction and wear

Figure 1 shows the friction coefficient recorded during the tests. For oil lubricated test, a low, reasonably constant, friction coefficient is observed (0.02 for brass and 0.04 for steel). The steel specimens were operating under higher load and therefore likely to have a thinner lubricant film and give a resulting higher friction coefficient. With water lubrication friction coefficients start low and then increase to a higher value (average of 0.18 in both cases). However the brass discs take many cycles to achieve this steady state value. It is likely that this incubation period is caused by the gradual roughening of the surface. Weight loss for rail steel discs is plotted in Figure 2 against number of rolling cycles under oil and water lubrication. It shows that the wear rate with water lubrication is much higher than in oil. In fact, the wear loss almost is negligible for oil case, only about 0.02 $mg/cycle$. For water lubrication, at these contact loads wear occurs by a process of ratchetting [22]. High tangential stress caused the build up of plastic strain in the direction of traction. Eventually the ductility of the material at the surface is exceeded and fracture occurs. A wear debris particle then detaches.

3.2 The shape of deformed defects

The size of the artificial indentations were monitored throughout the rail steel test. Figure 3 shows how the dent size (diameter for conical indent and diagonal length for pyramidal indent) varied with the number of loading cycles. In addition some sections through defects after testing were made. With an oil lubricated rail steel surface, the dent size showed an abrupt reduction (typically 50%) during the first few cycles and then remained virtually stable (see figure 3(a)). However the depth of the indentation remained unchanged. A similar trend was observed with brass oil lubricated surfaces. In this case dents were reduced in size by about 30% [19]. The transverse and longitudinal furrows in oil demonstrated a similar change i.e., a

distinct decrease in their width taking place during the first cycles and then reaching a stable stage.

Figure 4 shows the deformation of a conical dent on an oil lubricated brass surface. The bright spot indicates the original geometrical centre of the dent. As the dent is deformed it is clear that this original centre becomes off axis. Evidently the trailing edge of the dent has undergone more plastic flow and a greater change of dent shape. The deformation is therefore likely to be by flow in shear in the direction of the tractive force rather than by normal compressive loading.

For the water lubricated experiments the trend is somewhat different. In all cases, a stable shakedown dent is not formed and deformation continues until the mouth of the dent is closed (see figure 3(b)). The larger conical dents appeared the most resilient, and took around 60k cycles to be reduced to a small size. A similar test was carried out on a surface containing a drilled hole. A section through the hole (Figure 5) after running 42k cycles demonstrates that this disappearance of the dent is not due to wear of the surface but rather by plastic flow closing the dent mouth. Again under water lubricated condition, all the machined furrows observed to be closed up within 5k cycles for rail steel.

3.3 The characteristics of failure

3.3.1 Oil lubrication

The experiments show a clear influence of the presence of conical and pyramidal dents on cycling life. As shown in Figure 4 for brass, cracks and pits occurred around the conical dent. Most of them initiated a small distance from the trailing edge of the indentation. The initiation site is coincident with the location of the original dent edge. A 0.29 mm diameter spall was found after 240k cycles on the trailing edge of the conical dent. Rail steel undergoes a similar failure, as shown in Figure 6. A clear curved crack initiated at the trailing edge of a conical dent at 131k cycles (Figure 6(b)). It finally developed into a spall at 886k cycles (Figure 6(d)). The difference in failures between brass at 600 MPa and rail steel at 1500 MPa was that before the formation of a spall the brass surface showed many other locations of small pits and cracks. On steel surfaces there was only a single crack on the surface located at the dent edge. Generally larger dents cause a more rapid failure. However, in some tests, the effect of dent size is marginal. Interestingly, neither transverse nor longitudinal furrows had any influence on oil lubricated disc cycling life. No obvious pit or crack was observed around these furrows although they tended to be worn out after many cycles. The furrows are produced by machining whilst the conical and pyramidal defects are produced by indentation. It is thought that the raised dent edges associated with the latter cause high local shear stress and promote fatigue cracking. However, it should be noted that the furrows are relatively shallow and narrow and this may contribute to their negligible influence. Table 3 summaries the effect of defects on rolling fatigue life from the experimental results.

A clearer picture can be obtained from SEM examination of the specimen surface. Figure 7 shows a failed brass surface in the region of a pyramidal dent. Initially a long arrow-headed crack formed near the trailing edge of the pyramidal dent at 300k cycles. This developed into a large spall after a further 60k cycles. The three stages of forming a spall are; crack initiation, fast propagation and final shear lip of the crack, indicated as (b), (c), (d) in Figure 7(a), is shown respectively in Figures 7(b, c and d). A series of longitudinally sectioned surfaces around the above the dent have been examined to observe the morphology of the dent and spall underneath the surface. Figure 8 was taken near the centre the of the dent perpendicular

to the disc axis. This demonstrates that the spall, with a depth of 0.18 mm, is located just behind the trailing side of the pyramidal dent. A crack has propagated parallel to the disc surface and has formed the bottom of the spall. No cracks were observed to grow down into the material bulk.

3.3.2 Water lubrication

With water lubrication it was observed that dents had little influence on the life of rolling contact fatigue failure. Figures 9 and 10 show the sequence of typical test. The dent is deformed throughout the test and the dent mouth closes. There is no preferential cracking at the dent location. Even the largest conical dents and the drilled holes had no noticeable effect on the fatigue life. Figure 11 shows that transverse furrows have some slight influence on the failure. A network of cracks form along the original trailing edge of scratch and join together to form an extended crack (see Figure 11(d)). Cracks grew everywhere on the surface, most of them in the transverse direction. However this occurs at the same time as cracking on the surface remote from the scratch. The same does not occur in the case of longitudinal furrows (Figure 12). Cracks grow in the transverse direction and ignore the existence of a longitudinal furrow.

The sectioned surface revealed a different morphology between oil and water lubricated cases. As shown in Figure 13, for rail under water lubrication, the inclined cracks grew deep into the specimen with much branching. The crack propagation direction was opposite to the direction of traction. In general, the crack initiates at the contact surface and starts to propagate at an angle of around $5°$ to the surface. During the first stage it propagates through the surface deformation zone (about $10\,\boldsymbol{mm}$ deep). Then the crack turns downwards by a further 25-$35°$ and grows to a depth of around 300-400 $\boldsymbol{mm}$. The branches of crack appear to grow at around $90°$ to the main crack. The depth of cracking was seen to be about $500\,\boldsymbol{mm}$. This is a typical kind of surface cracking observed with water lubricated rolling contact [20, 21]. Clearly, crack growth deep into surface is the dominant feature of water lubricated contacts rather than the spall failure observed under oil lubrication.

3.4 Hardness measurements

Figure 14(a) shows the strain hardening behaviour beneath the rail disc contact surface after testing. It can be seen that the depth of maximum hardening is below the surface. The depth of the work-hardened layer is about 1.3 mm and the maximum hardness is about 1.4 times the initial hardness. The depth of measured hardness increase is greater than the depth of the heavily sheared zone (about 0.5 mm) observed using microscopy. Water or oil lubrication has no obvious effect on the depth of maximum hardening. The magnitude of the hardness reached and the depth of the work-hardened layer increases with increasing contact pressure. There is no apparent hardness change below the contact surface for brass at 600 MPa and only a slight increase in hardness value for brass at 750 MPa (see Figure 14(b)) and for rail at 900 MPa.

4. DISCUSSION

4.1. Fluid film thickness

Although mechanical and metallurgical factors such as contact stress, residual stress, presence of inclusions, and other imperfections in the materials are often reported to be among the most important factors controlling fatigue, research work has demonstrated that the change of lubrication condition can vary the fatigue life of engineering components [23]. A lubricating oil film can act to separate the running surfaces and reduce the coefficient of traction, but it can also act to pressurise a crack and promote propagation.

In the oil lubricated tests an elastohydrodynamic oil film will be formed. The thickness of the film may be determined from the linear regression equation of Dowson and Higginson [24]:

$$H_{min} = 2.65 G^{0.54} U^{0.7} W^{-0.13} \tag{1}$$

where $H_{min} = h_{min}/R$

$$G = 2aE^{*}$$

$$U = \bar{U} h_{\circ} / 2E^{*} R$$

$$W = \bar{W} / 2E^{*} R L$$

When the discs are lubricated with water these equations are no longer suitable. Chen et. al [25] have developed a similar approach based on numerical results with low viscosity fluid lubricants:

$$H_{min} = 2.578 G^{0.002} U^{0.597} W^{-0.211} \tag{2}$$

For water an equivalent pressure viscosity coefficient $a' = 0.683 \; GPa^{-1}$ is used. Using these two methods for determining the lubricant film thickness gives the results in Table 4.

When the film thickness is less than the combined roughness of the surface it can have a significant effect on stress concentration and surface damage. It has been recognised that Λ is one of the parameters which influences fatigue life [6, 15, 26].

$$\Lambda = \frac{h_{min}}{\sqrt{s_1^2 + s_2^2}} \tag{3}$$

where s_1 and s_2 represent the RMS surface roughness of the driven and the driving disc. Table 4 shows the film thickness parameter for the tests carried out in this study. Thus, with thick elastohydrodynamic films, the infrequent asperity contacts lead to reduced traction and a low probability of crack formation. As asperity contact increases with decreasing film thickness, cracks are formed more readily and in greater numbers [27]. The experimental results by Cheng [15] have revealed that when the film thickness parameter Λ is smaller than 0.3, cracks are initiated everywhere on the surface, and when Λ is greater than 0.5, no surface cracks could be found, except at the region near the surface defects [15, 16, 28]. This is consistent with our experimental results: when $\Lambda < 0.017$ in the water lubricated case without appropriate film protection, surface cracks grow everywhere (see Figures 9-12); and when $\Lambda > 1.3$ in oil lubricated case, cracks only initiate near the defect (see Figures 4 and 6), where the film profile is affected by the existence of the defects.

It has been demonstrated [29] that a debris dent on an otherwise smooth contact surface can significantly modify the film thickness (and hence the stress concentration). Film thickness measurements associated with a debris dent have been made by interferometry under static and dynamic conditions [12, 29]. The results show that the film thickness is slightly different for the leading and trailing edges of the dent. Wedeven [12] explained that the greater slope at the leading edge of the dent should be less favourable for pressure generation than the trailing edge where the slope is in the opposite direction. As a result, the trailing edge suffers more pressure and stress concentration. This maybe the reason why there is more damage at the trailing edges of dents than at the leading edges in the present oil lubricated experiments.

4.2. Lubricant in the crack and the hydraulic pressurisation mechanism

It has been widely stated that liquid can influence fatigue crack growth in a number of ways: it may reduce the friction forces acting between the faces of the crack; it may squeezed into the crack by the passing load; or it may be trapped inside the crack and forced towards the crack tip [1, 30].

Without the presence of a lubricant it is thought that the crack faces stick under load and that the only propagation mechanism is by the action of relatively low shear stresses (i.e. mode II). However when the fluid is present and the hydraulic pressurisation mechanism occurs, much more rapid mode I propagation is possible. It is important to note that the presence of water can have a further deleterious effect (in addition to hydraulic pressurisation and low film thickness). Water as a contaminant in a mineral oil is known to reduce contact fatigue life and this effect increases with concentration [31, 32]. The main effect of water, however, is on crack propagation due to its physical and chemical properties. For example, the high pressure viscosity coefficient in mineral oils results in a large increase in viscosity of the fluid at the mouth of a newly initiated crack so isolating the growing crack tip from the high pressure pulse. Water remains at low viscosity and thus transmits the pressure to the growing tip.

Sullivan [27] explained the influence of water on crack propagation rate as originating from two effects. One is mechanical, where a greater volume of fluid is more likely to maintain the high compressive stress necessary for rapid crack growth. The other is chemical, where, according to Scott [33], water-produced hydrogen diffuses into the highly stressed material ahead of the microcracks resulting in hydrogen embrittlement. Polk and Rowe [34, 35] found, by using an optical method, that lubricant chemical factors affected fatigue life by influencing the crack branching rate.

In addition, the effect of water and oil lubrication can be different for each of the two modes of crack growth [36]. Oil is more effective in reducing friction of the initial shear crack faces while water would penetrate to the crack tips more easily in branch cracking. As a result, surface cracks do not propagate beyond the work hardened surface layer with oil, whereas the water lubrication results in much deeper branched crack networks. This is consistent with our experimental results in which pits or a spall are restricted to a near surface region with oil lubrication but in water cracks grow deep into the surface, as shown in Figures (8 and 13).

In reviewing published rolling contact fatigue literature over the past twenty years, most engineering elements with spall related failures occurred under oil lubrication (bearings and gears etc.) [37, 38]. Whilst most crack related failures took place under water lubrication, such as rail-wheel contact [20, 21, 36]. This may emphasise that the mechanism of cracking or spalling is strongly dependent on the lubrication condition. Pure spalling failure without any

surface fatigue phenomenon signifies extremely good lubrication and predominant surface fatigue signifies inferior lubrication [38].

4.3. Stress intensity factor and coefficient of traction

A lubricated rolling/sliding line contact system which contains surface breaking cracks has been simulated by Kaneta et al [39]. The elastic half-space containing a surface crack inclined to the half-space surface is loaded by a Hertzian contact pressure distribution. The normal and tangential surface stresses are defined as follows:

$$p(x) = p_0(1 - x^2/c^2)^{1/2} \tag{4}$$

$$q(x) = \boldsymbol{m}p(x) \tag{5}$$

where $\boldsymbol{m}$ is mean coefficient of surface traction and c is the radius of the area of contact. The stress intensity factors which represent the intensities of the fields of shearing stress $\boldsymbol{t}_{rq}$ and tensile stress $\boldsymbol{s}_q$ near the crack tip are expressed as follows:

$$K_t(\boldsymbol{q}) = \boldsymbol{t}_{rq}\sqrt{2\boldsymbol{pr}} = \frac{1}{2}\cos\frac{\boldsymbol{q}}{2}\left[K_I \sin\boldsymbol{q} + K_{II}(3\cos\boldsymbol{q} - 1)\right] \tag{6}$$

$$K_s(\boldsymbol{q}) = \boldsymbol{s}_q\sqrt{2\boldsymbol{pr}} = \cos\frac{\boldsymbol{q}}{2}\left[K_I \cos^2\frac{\boldsymbol{q}}{2} - \frac{3}{2}K_{II}\sin\boldsymbol{q}\right] \tag{7}$$

where $(r,\boldsymbol{q})$ indicates the polar co-ordinate systems, the origin of which is located at crack tip.

It is shown [39] that when a crack is small, the maximum tensile stress intensity factor $K_{\boldsymbol{s}\,max}$ is much smaller than the threshold stress intensity factor range $\Delta K_{\boldsymbol{s}th}$ during a loading cycle. Conversely, maximum shear stress intensity factor $K_{\boldsymbol{t}\,max}$ has a relatively large value when the crack is closed. Therefore, it is expected that the crack growth occurs along the original crack plane by shear mode. If we assume a small crack of length, a, where $a/c = 0.1$ angled at $45°$, published stress intensity factor data is available [40, 41]. The data is presented in non-dimensional form:

$$\Delta K_{\boldsymbol{t}\,max} = \Delta F_{\boldsymbol{t}\,max}\, p_0\sqrt{\boldsymbol{p}a} \tag{8}$$

where $\Delta F_{\boldsymbol{t}\,max}$ is tabulated for various crack length, angles and friction coefficients. For a surface traction coefficient of 0.04 (corresponding to the oil lubrication tests) and a contact pressure $p_0 = 1500$ MPa, the maximum shear stress intensity factor range is calculated as $\Delta K_{\boldsymbol{t}\,max} = 1.06\, MPa\sqrt{m}$. The threshold stress intensity factor is approximately $\Delta K_{tth} \approx 1.5\, MPa\sqrt{m}$ [42], so a crack is not expected to propagate in this condition without the presence of further stress raising defects.

Repeating this calculation for the water lubricated case, where $\boldsymbol{m} = 0.18$ gives $\Delta K_{\boldsymbol{t}\,max} = 2.75\, MPa\cdot\sqrt{m}$. This value exceeds the threshold and thus we would expect shear mode growth to occur.

From the above results, it can be concluded that a microcrack may propagate by shear mode only when sufficient surface traction exists. The reason is that the contact pressure gives rise

to large compressive stress field in the neighbourhood of the contact region, therefore, the crack growth is unlikely to occur without sufficient surface traction [43]. In addition, the surface traction is the controlling factor for lubricant seepage into the crack and for shear mode crack growth rate. The analytical results support the hypothesis that a crack first propagates in shear, and that crack growth by tensile mode follows due to a hydraulic effect on crack faces by the lubricant that has penetrated into the crack [39, 44].

The formation of a surface arrow headed crack has been studied by a numerical technique [44]. This analysis showed that the arrow headed crack spread angle b, experimentally observed on the contact surfaces under rolling contact fatigue tests, was strongly influenced by the load condition and the frictional force. According to the analytical results, the spread angle, b, of a crack increases with increasing the frictional force. Therefore, it is possible to estimate the operating conditions of contact loading by comparing the observed spread angle of a crack on the contact surface. The present experimental results have showed that a large crack spread angle occurs in the high traction water lubricated case (see Figures 9-12(d)). A small crack spread angle occurs in low traction oil lubricated case (see Figures 4(c) and 6(c)). A schematic explanation of effect of the traction on crack spread angle is shown in Figure 15. The top view in Figure 15 shows that the effect of traction on b, and the cross section shows that high traction is often associated with deep branch cracks and low traction is associated with a single spall which has a depth less or equivalent with maximum shear stress, as shown in Figures 8 and 13. Also noted is that in cases of high traction there are usually many cracks perpendicular to the rolling direction on the disc surface. Conversely, there are only few isolated arrow-headed cracks on the disc surface in the cases of low traction (as shown in Figures 9-12 and Figures 4 and 6).

4.4. Hardening depth

From Figure 14(a), it can be seen that the peak hardness value with 1500 MPa is at 0.18-0.23 mm below the contact surface. This figure is close to the depth of maximum shear stress, t_1, of 0.24 mm, which has been estimated from an elastic Hertzian analysis.

In oil lubricated cases we observe the crack propagating close to this depth of maximum shear stress. For example, in brass at 600 MPa, the calculated depth of maximum principal shear stress is $177\,mm$, which is close to the depth of $180\,mm$ at which the spall propagates, shown in Figure 8. Ai and Lee [46] obtained a similar experimental result in which the spall started with a crack initiating near the surface at the trailing edge and propagating downward to the depth of the maximum stress in a Hertzian contact. The crack would then turn and propagate parallel to the surface, and finally turn up to form a spall. In water, however, no correlation was observed between the maximum shear stress and the regions of crack propagation.

An important observation in this work was the absence of a difference in the sub-surface work hardening under water and oil lubricated cycling under the same contact pressure (Figure 14(a)). This means that simply using work hardening as a measure of the damage in the material is inadequate to describe the fatigue behaviour. This phenomena has also been found in the cases with or without a reversal in the direction of the test [21].

In addition, comparing with Figures 14(a) and 14(b), it is showed clearly that there is much more working hardening in rail steel than in brass though they are tested under comparable ratio of p_0/H. This may partly explain why there are more small cracks and pits around

indentation in brass (Figure 4(c)) than in rail steel (Figure 6(c)) because of their different capacity for plastic deformation and strain hardening.

5. CONCLUSIONS

A study into effects of surface defects on rolling contact fatigue of brass and rail steel under maximum contact pressure of 600-1500 MPa and a slide-roll ratio of -1% was undertaken on a twin-disc rolling-sliding test machine with oil and water lubrication. Furrows (transverse and longitudinal) and dents (conical and pyramidal) were artificially introduced into the disc surfaces. The surface micro cracks and pits were monitored by means of surface replication throughout the tests.

1. Under oil lubrication, the dent showed a rapid size reduction of about 40-50 % and then remained virtually stable with further cycling. With water lubrication, the dent size decreased continuously throughout the test until closure of the dent mouth occurred.

2. With oil lubrication, an obvious influence of conical and pyramidal dents on cycling life has been demonstrated. However, neither transverse nor longitudinal furrows had any influence on disc cycling life. The furrows were created by a material removed process and, unlike the indentation, has no raised shoulders. This is thought to be the reason for the difference in fatigue effect. The relatively narrow width and shallow depth in furrows considered here maybe is another reason.

3. With water lubrication, the dents and longitudinal furrows did not have any influence on the life of the contact. The whole of the surface exhibits cracking with no particular disposition towards the region of the indentation. Transverse furrows promoted some surface crack networking and so demonstrated a minor influence on contact life.

4. The presence of a surface indentation modifies the local elastohydrodynamic film. The pressure and stress concentration at the trailing edge of the defect is increased. This results in most oil lubricated failures occurring at the trailing edge of the defects.

5. Oil is more effective in reducing crack face friction while water is able to penetrate to the crack tip more easily. In water lubricated cases, surface cracks grew everywhere on the surface. With oil lubricated case, failure occurred at an indentation. The increased traction and fluid penetration of the water lubrication is thought to be the origin of these differences.

6. The formation of a surface spall, propagating in the region of the depth of maximum shear stress, is characteristic of an oil lubricated failure. Deep branched cracks are formed with water lubrication.

7. It is possible to estimate the operating conditions of contact loading by comparing the observed spread angle of a crack on the contact surface. A large crack spread angle corresponds to a large surface traction and a small crack spread angle corresponds to a small surface traction.

REFERENCES

1. **Way, S.** Pitting due to rolling contact. *J. Applied Mech., Trans. ASME*, 1935, **2**, 49-58.

2. **Lubrecht, A. A.** and **Ioannides, E.** A Fast Solution of the Dry Contact Problem and the Associated Sub-Surface Stress Field, using Multilevel Techniques. *Transactions of the ASME, Journal of Tribology*, 1991, **113**, 128-133.

3. **Lundberg, G.** and **Palmgren, A.** Dynamic capacity of rolling bearings. *J. Applied Mech., Trans. ASME*, 1949, **16**, 165-172.

4. **Merwin, J. E.** and **Johnson, K. L.** An analysis of plastic deformation in rolling contact. In *Proc. Instn. Mech. Engrs. Symp on Fatigue in Rolling Contact*, 1963, 145-154.

5. **Dawson, P. H.** Effect of metallic contact on the pitting of lubricated rolling surfaces. *J. Mech. Engg. Sci.*, 1962, **4**, 16-21.

6. **Liu, J. Y., Tallian, T. E.** and **McCool, J. I.** Dependence of bearing fatigue life on film thickness to surface roughness ratio. *ASLE Transactions*, 1975, **18**, 144-152.

7. **Muro, H., Tsushima, T.** and **Nagafuchi, M.** Initiation and propagation of surface cracks in rolling fatigue of high hardness steel. *Wear*, 1975, **35**, 261-282.

8. **Olver, A. V.** and **Spikes, H. A.** The residual stress distribution in a plastically deformed model asperity. *Wear*, 1986, **107**, 151-174.

9. **Soda, N.** and **Yamamoto, T.** Effect of tangential traction and roughness on crack initiation/propagation during rolling contact. *ASLE Transactions*, 1982, **25**, 198-206.

10. **Lubrecht, A. A., Dwyer-Joyce, R. S.** and **Ioannides, E.** Analysis of the influence of indentations on contact life. In *Proc. of 18th Leeds-Lyon Symposium on Tribology* (Eds D. Dowson, C. M. Taylor and M. Godet), 1991.

11. **Martin, J. A.** and **Eberhardt, A. D.** Identification on potential failure nuclei in rolling contact fatigue, *ASME Journal of Basic Engineering*, 1967, **89**, 932-942.

12. **Wedeven, L. D.** and **Cusano, C.** Elastohydrodynamic film thickness measurements of artificially produced surface dents and grooves, *ASLE Transactions*, 1979, **22**, 369-381.

13. **Cusano, C.** and **Wedeven, L. D.** Elastohydrodynamic film thickness measurements of artificially produced non-smooth surfaces, *ASLE Transactions*, 1981, **24**, 1-14.

14. **Cusano, C.** and **Wedeven, L. D.** The effects of artificially-produced defects on the film thickness distribution in sliding EHD point contacts, *ASME Journal of Lubrication Technology*, 1982, **104**, 365-375.

15. **Cheng, W., Cheng, H. S.** and **Keer, L. M.** Longitudinal crack initiation under pure rolling contact fatigue, *Tribology Transaction*, 1994, **37**, 51-58.

16. **Cheng, W., Cheng, H. S.** and **Keer, L. M.** Experimental investigation on rolling/sliding contact fatigue crack initiation with artificial defects, *Tribology Transaction*, 1994, **37**, 1-12.

17. **Yoshimura, H., Rubin, C. A.** and **Hahn, T. G.** A technique for studying crack growth under repeated rolling contact. *Wear*, 1984, **95**, 29-34.

18. **Chen, L. C., Qing, C.** and **Shao, E. Y.** Study on initiation and propagation angles of subsurface cracks in GCr15 bearing steel under rolling contact. *Wear*, 1989, **133**, 205-218.

19. **Gao, N., Dwyer-Joyce, R. S.** and **Beynon, J. H.** Effects of surface defects on rolling contact fatigue of 60/40 brass. *Wear*, 1999, **225-229**, 983-994.

20. **Beynon, J. H., Garnham, J. E.** and **Sawley, K. J.** Rolling contact fatigue of three pearlitic rail steels. *Wear*, 1996, **192**, 94-111.

21. **Tyfour, W. R.** and **Beynon, J. H.** The effect of rolling direction reversal on fatigue crack morphology and propagation. *Tribology International*, 1994, **27**, 273-282.

22. **Tyfour, W. R., Beynon, J. H.** and **Kapoor, A.** Deterioration of rolling contact fatigue life of pearlitic rail steel due to dry-wet rolling-sliding line contact. *Wear*, 1996, **197**, 255-265.

23. **Founds, F. G.** Effects of base oil viscosity and type on bearing ball fatigue. *ASLE Transactions*, 1962, **5**, 172-182.

24. **Williams, J. A.** *Engineering Tribology*, 1994, (Oxford University Press).

25. **Chen, H., Yoshimura, A.** and **Ohyama, T.** Numerical analysis for the influence of water film on adhesion between rail and wheel. *Proc. Instn. Mech. Engrs.,* 1998, **212**, 359-368.

26. **Tallian, T. E.** and **McCool, J. I.** An engineering model of spalling fatigue in rolling contact, II. The surface model. *Wear*, 1971, **17**, 447-461.

27. **Sullivan, J. L.** and **Middleton, M. R.** The pitting and cracking of SAE 52100 steel in rolling/sliding contact in the presence of an aqueous lubricant. *ASLE Transactions*, 1985, **28**, 431-438.

28. **Zhai, X. J.** and **Chang, L.** On mechanisms of fatigue life enhancement by surface dents in heavily loaded rolling line contact. *Tribology Transaction*, 1997, **40**, 708-714.

29. **Wedeven, L. D.** Influence of debris dent on EHD lubrication, *ASLE Transactions*, 1978, **21**, 41-52.

30. **Bower, A. F.** The influence of crack face friction and trapped fluid on surface initiated rolling contact fatigue cracks, *Transactions of the ASME, Journal of Tribology*, 1988, **110**, 704-711.

31. **Armstrong, E. L., Leonardi, S. J., Murphy, W. R.** and **Wooding, P. S.** Evaluation of water-accelerated bearing fatigue in oil lubricated ball bearings. *Lubrication Engineering*, 1978, **34**, 15-21.

32. **Woodger, G. B.** Progress towards the introduction of HWBF hydraulic fluids. *Auto. Man. Update '81, Con. Mech. Eng. Pub.*, C278/81, 1981, 33.

33. **Scott, D.** The effect of material properties, lubricant and environment on rolling contact fatigue. In *Proc. Symp. Fatigue in Rolling Contact, I. Mech. E.*, 1963, 103-115.

34. **Polk, C. J., Murphy, W. R.** and **Rowe, C. N.** Determining fatigue crack propagation rates in lubricating environments through the application of a fracture mechanics technique. *ASLE Transactions*, 1975, **18**, 290-298.

35. **Polk, C. J.** and **Rowe, C. N.** Crack growth rate: Its measurement and a controlling factor in rolling contact fatigue. *ASLE Transactions*, 1976, **19**, 23-32.

36. **Clayton, P.** and **Su, X.** Surface initiated fatigue of pearlitic and bainitic steels under water lubricated rolling/sliding contact. *Wear*, 1996, **200**, 63-73.

37. **Tallian, T. E.** *Failure Atlas for Hertz Contact Machine Elements*, 1992, (ASME Press, New York).

38. **Tallian, T. E.** On competing failure modes in rolling contact, *ASLE Transactions*, 1967, **10**, 418-439.

39. **Kaneta, M., Yatsuzuka, H.** and **Murakami, Y.** Mechanism of crack growth in lubricated rolling/sliding contact. *ASLE Transactions*, 1985, **28**, 407-414.

40. **Kaneta, M., Murakami, Y.** and **Yatsuzuka, H.** Propagation of surface crack in rolling line contact. In *Proc. JSLE Int. Tribology Conference*, Tokyo, Japan, 1985, 911-916.

41. **Murakami, Y.** *Stress Intensity Factors Handbook*, Volume 2, 1990, (Pergamon Press).

42. **Otsuka, A., Mori, K.** and **Miyata, T.** The condition of fatigue crack growth in mixed mode condition. *Eng. Fracture Mech.*, 1975, **7**, 429-439.

43. **Murakami, Y., Sakae, C., Ichimaru, K.** and **Kaneta, M.** Elastic-plastic analysis of subsurface layer under cyclic rolling-sliding contact loading and pit formation mechanism. In *Advances in Engineering Tribology* (Ed. Y. W. Chung), STLE. SP-31, 1991, 71-88.

44. **Murakami, Y., Sakae, C.** and **Ichimaru, K.** Three-dimensional fracture mechanics analysis of pit formation mechanism under lubricated rolling-sliding contact loading. *Tribology Transaction*, 1994, **37**, 445-454.

45. **Timoshenko, S. P.** and **Goodier, D. N.** *Theory of Elasticity*, 1970, (McGraw-Hill, New York).

46. **Ai, X.** and **Lee, S. C.** Effect of slide-to-roll ratio on interior stresses around a dent in EHL contacts, *Tribology Transaction*, 1996, **39**, 881-889.

Table 1. Chemical composition and mechanical properties of the test materials

Materials	Rail	Wheel	Brass	
Chemical Composition (wt%)				
C	0.73	0.50	Cu	57.9
Si	0.29	0.21	Sn	0.06
Mn	1.06	0.79	Pb	2.52
Ni	0.02	0.08	Ni	0.09
Cr	0.02	0.08	Fe	0.05
S	0.02	0.048	Zn	Rem.
P	0.016	0.016		
Mo	<0.02	<0.02		
Cu	<0.02	0.23		
Mechanical properties				
Average hardness (HV 20kg)	262	191	131	
Yield stress (MPa)	443	318	222	
Elongation to failure (%)	9.5	17.8		
Reduction in area (%)	22.7	36.9		
Young's Modulus (GPa)	210	210	110	
Poisson's ratio	0.3	0.3	0.34	

Table 2. Test conditions

Test Materials	60/40 brass, rail and wheel steels
Initial Surface Roughness, (R_a, μm)	0.35
Types of Surface Defects	Furrow (Transverse and Longitudinal) and Dents (Conical and Diamond)
Maximum Contact Pressure (MPa)	600 - 1500
Slide-Roll Ratio (%)	-1
Test Speed (RPM)	397(Driven disc)/402(Driving disc)
Lubrication	Water (one drip per second) Oil (one drip per 3 second)

Table 3. Summary of experimental results on the effect of defects on rolling contact life with oil and water lubrication

Material	p_0 MPa	Lubrication	Defect	Defect size		Effect (Y/N)	Life, Cycles	Location of failure
				Before test, mm	Reduction after test, %			
Brass	600	Oil	●	0.2-0.3 0.45-0.55	25-30 28-29	Y	>700k 230-240k	At trailing edge
			◆	0.2-0.3 0.45-0.55	47-50 29-36	Y	>700k 360-600k	At trailing edge
			—	0.1-0.3	50-53	N	>700k	
			|	0.1-0.2	75-80	N	>700k	
			No defect	-	-	-	>700k	All over surface
Brass	750	Water	●	0.6-1.1	100	N	32k	All over surface
			◆	0.5-1.2	100	N	32k	All over surface
			—	0.09-0.13	100	N	32k	All over surface
			|	0.03-0.13	100	N	32k	All over surface
			No defect	-	-	-	32k	All over surface
Rail steel	1500	Oil	●	0.45-0.65 0.76-1.2	52-65 40-57	Y	>1000k 700-900k	At trailing edge
			◆	0.34-0.55 0.70-1.1	49-56 27-41	Y	>800k 300-700k	At trailing edge
			—	0.21-0.26	23-24	N	> 1000k	
			|	0.025-0.08	60-88	N	> 1000k	
			No defect	-	-	-	> 1000k	All over surface
Rail steel	1500	Water	●	0.48-0.70 0.8-1.06	100 64-88	N	50k	
			◆	0.17-0.98	100	N	50k	
			—	0.21-0.27	100	Y	35-40k	Along scratch
			|	0.11-0.16	100	N	50k	
			No defect	-	-	-	50k	All over surface

16

Table 4 Film thickness parameters under oil and water lubrication

	Oil		Water	
	h_{min}, $\mathbf{m}m$	Λ, $\mathbf{m}m$	h_{min}, $\mathbf{m}m$	Λ, $\mathbf{m}m$
Brass at 600 MPa	0.82	1.66	0.0082	0.017
Rail steel at 1500 MPa	0.69	1.39	0.005	0.010
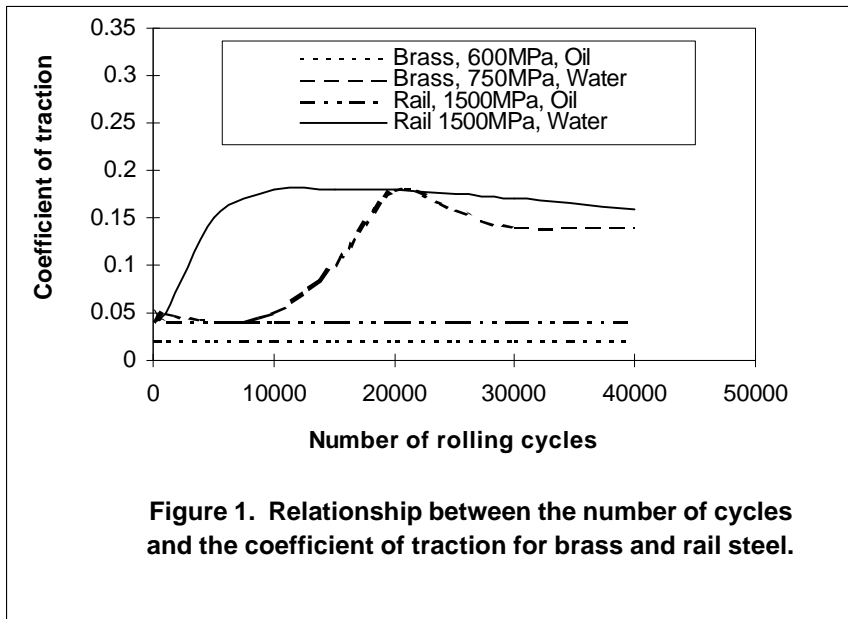
Figure 1. Relationship between the number of cycles and the coefficient of traction for brass and rail steel.
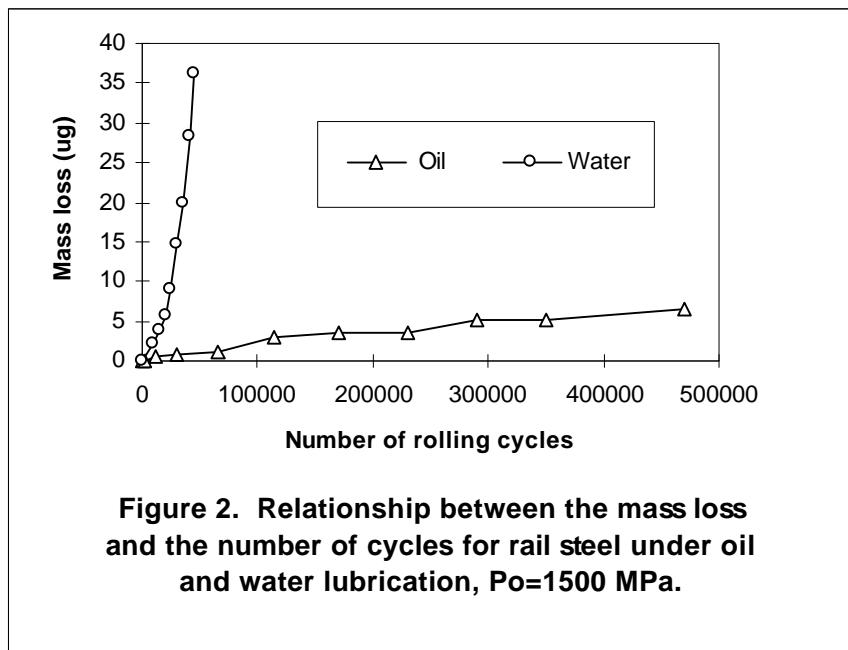
Figure 2. Relationship between the mass loss and the number of cycles for rail steel under oil and water lubrication, Po=1500 MPa.
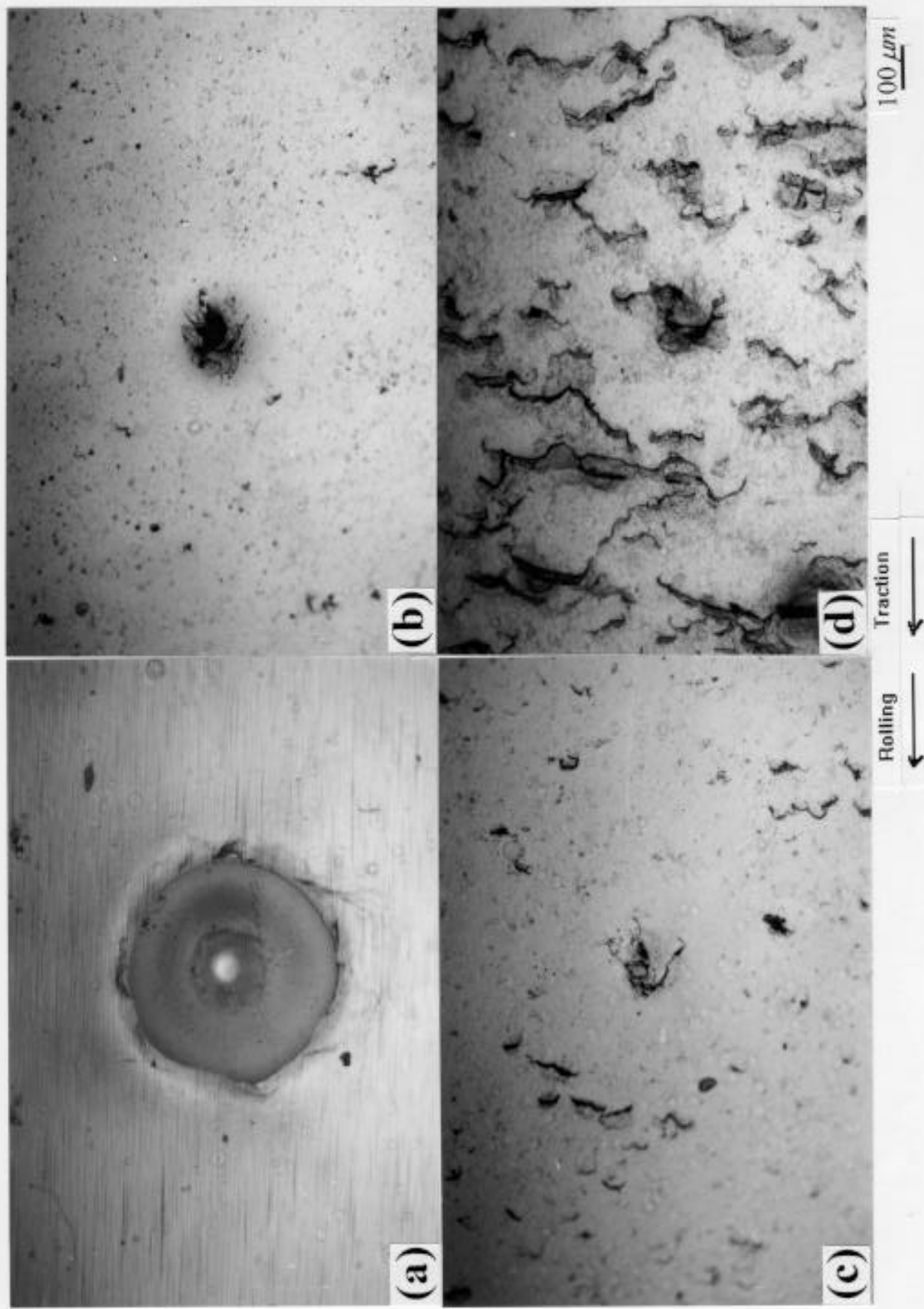
(a)

rail, Po=1500 MPa. (a) Oil; (b) Water.
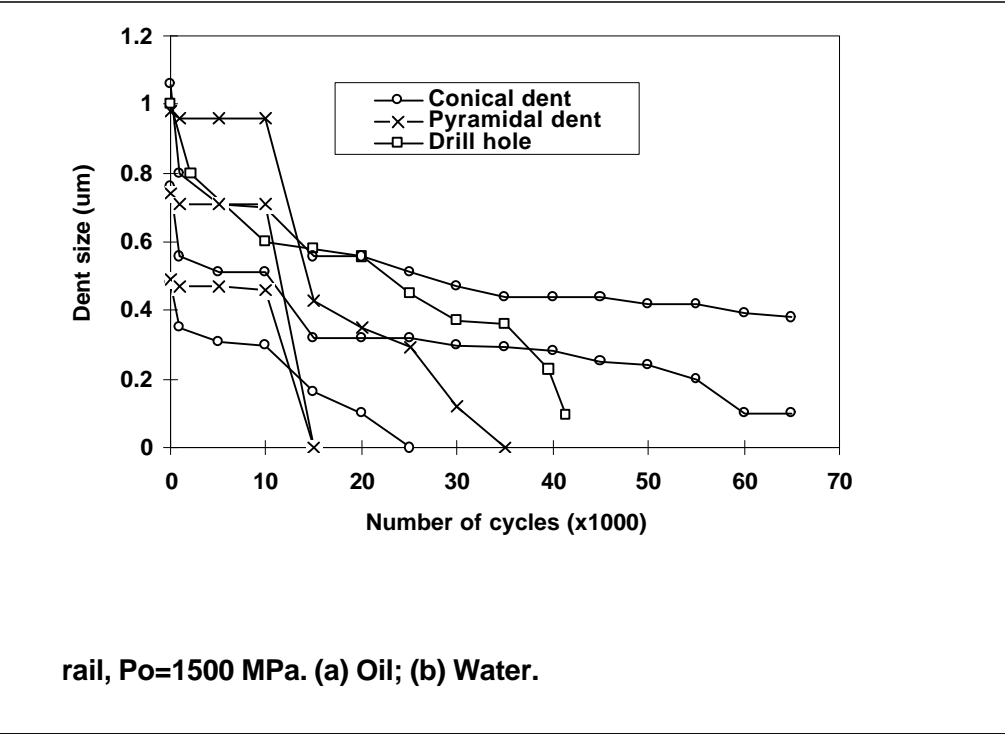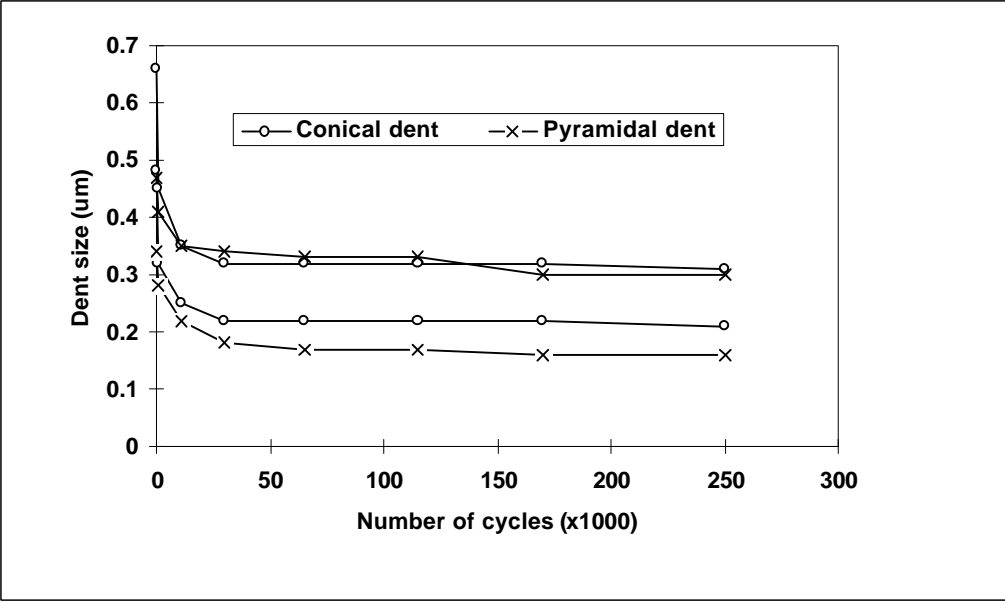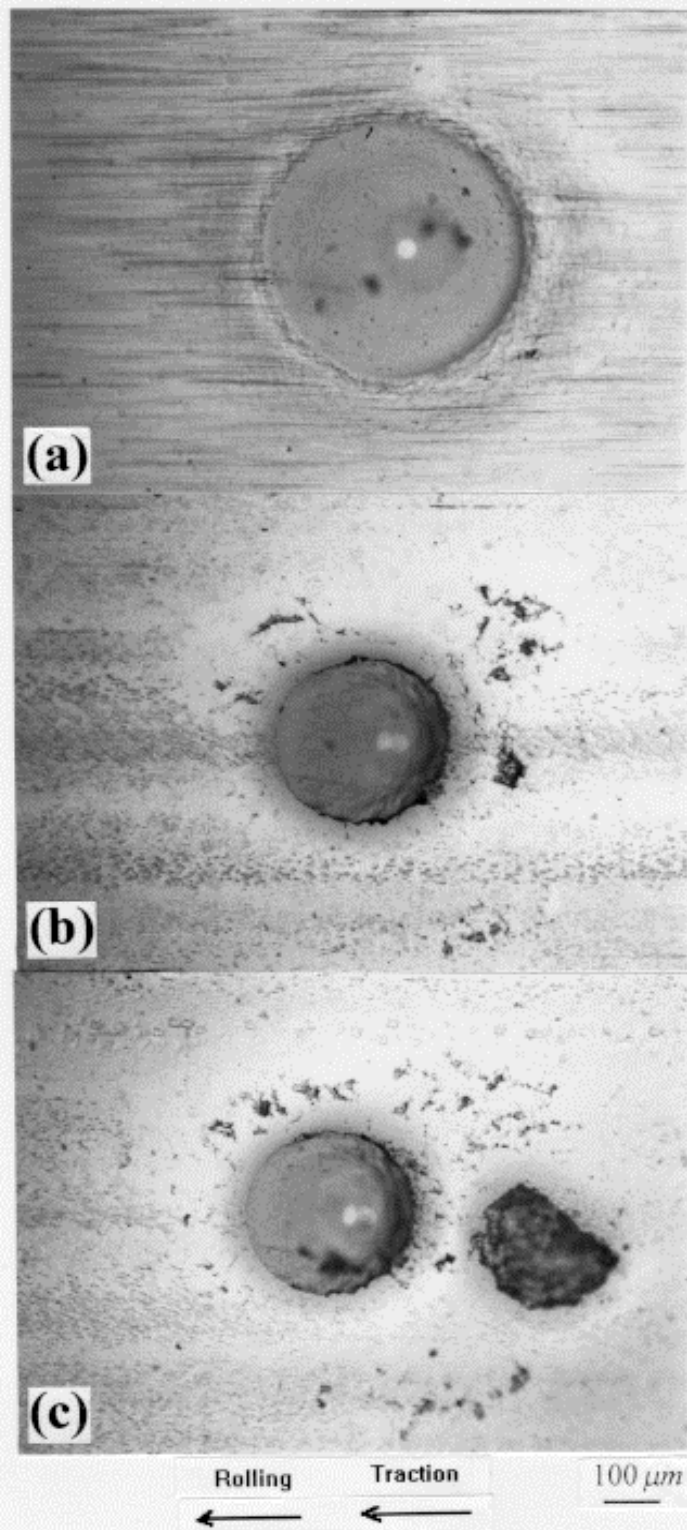
Figure 4. Progression of damage on the disc surface of brass around a conical dent, $p_0 = 600$ MPa , oil lubrication. (a) N = 0; (b) N = 120k; (c) N = 240k cycles.
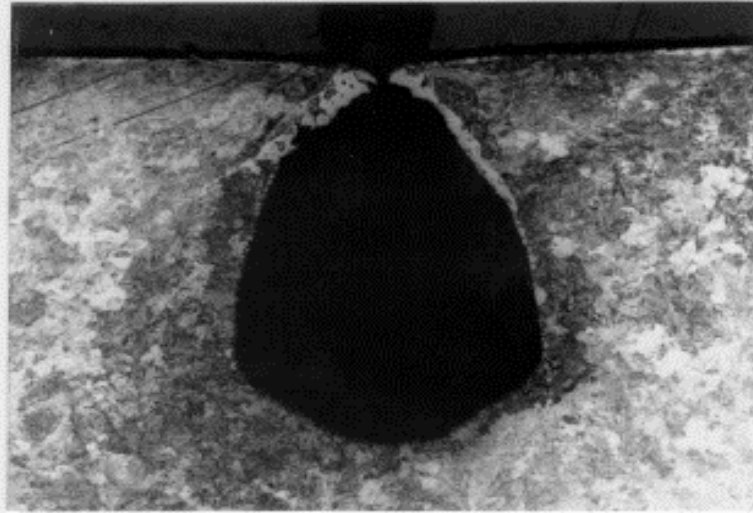
200 μm

Figure 5. Transverse section through a drilled hole in a rail steel disc after 42k
cycles of oil lubrication. The mouth of the hole is closed by repeated
plastic flow.
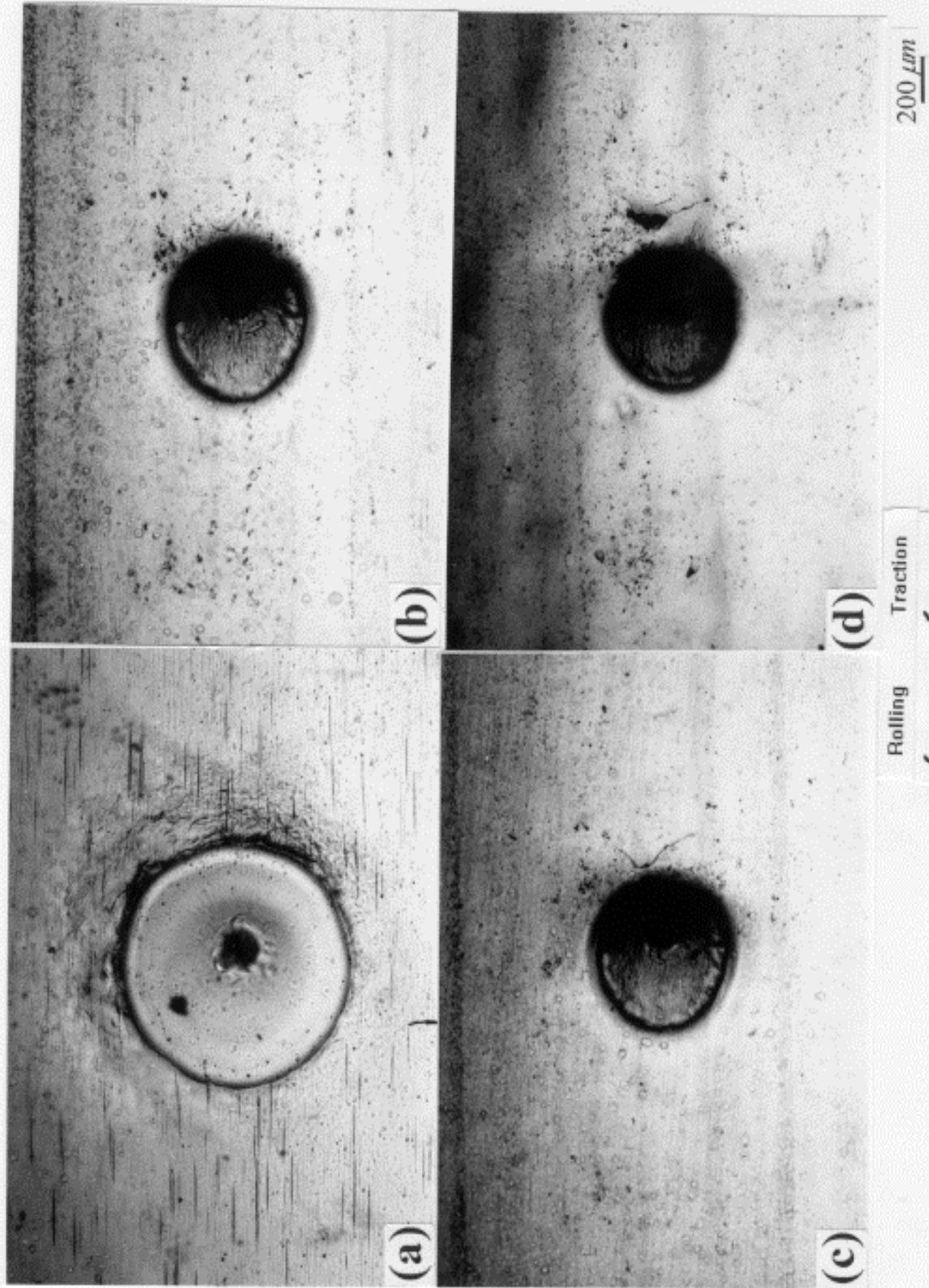
Figure 6. Progression of damage on the disc surface of rail around a conical dent, $p_0 = 1500$ MPa , oil lubrication.

(a) $N = 0$; (b) $N = 131$k; (c) $N = 465$k; (d) $N = 866$k cycles.
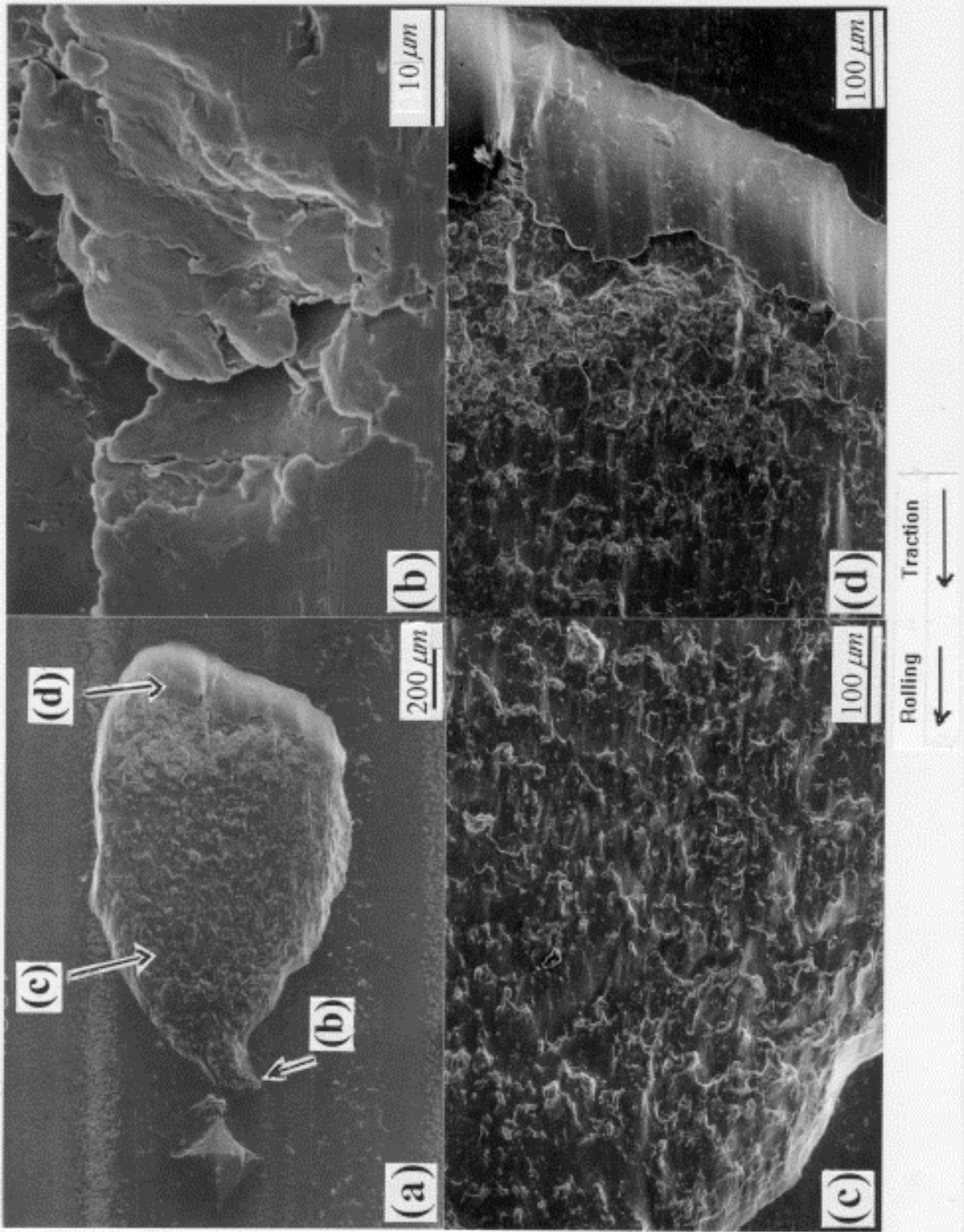
Figure 7. Morphology of spall formation around a pyramidal dent, brass, p_0 = 600 MPa, oil lubrication. (a) view of the failure surface; (b) spall initiation site; (c) spall fast propagation area; (d) final shear lip of spall.

Figure 8. Morphology of the pyramidal dent and spall observed from a longitudinally sectioned brass oil lubricated surface, $p_0 = 600$ Mpa.
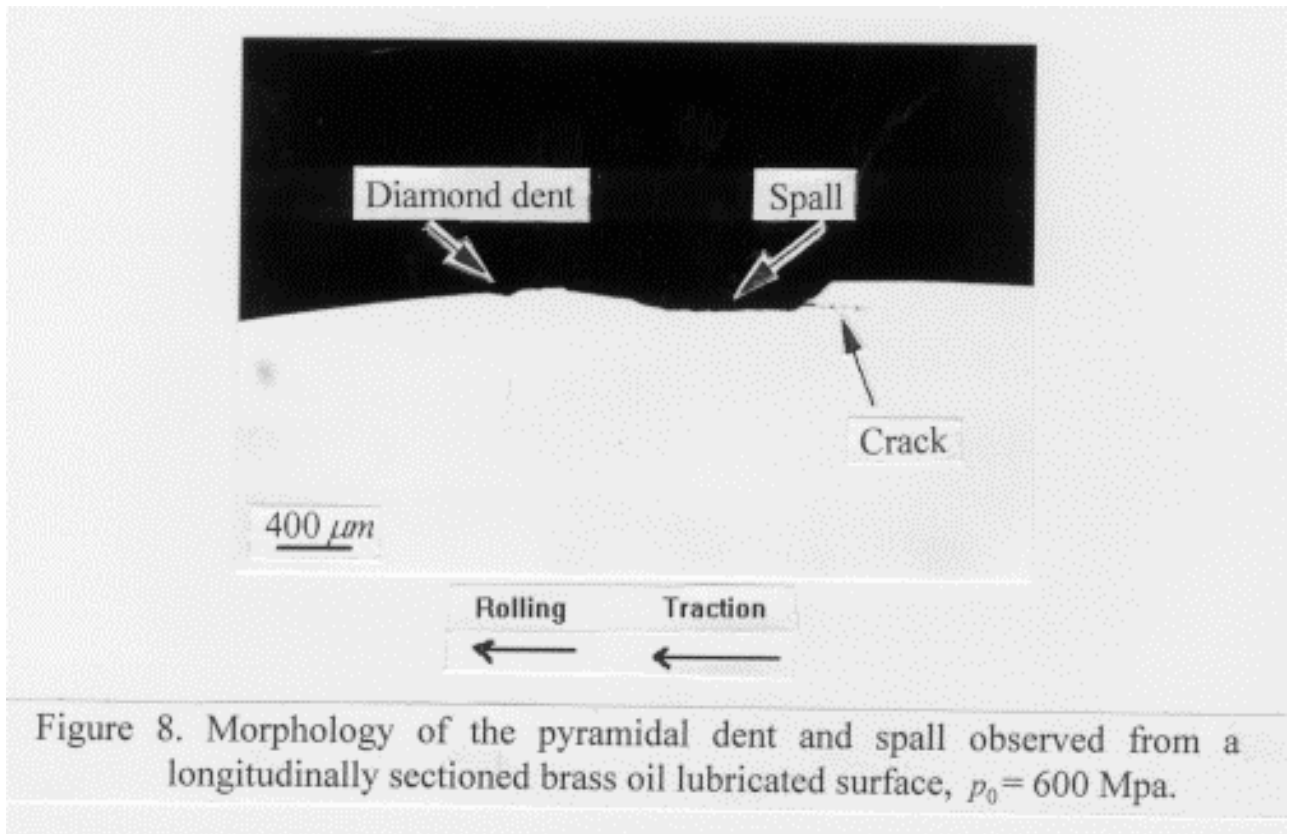
Figure 9. Progression of damage on the disc surface of rail around a conical dent, $p_0 = 1500$ MPa , water lubrication.

(a) N = 0; (b) N = 10k; (c) N = 20k; (d) N = 40k cycles.

24
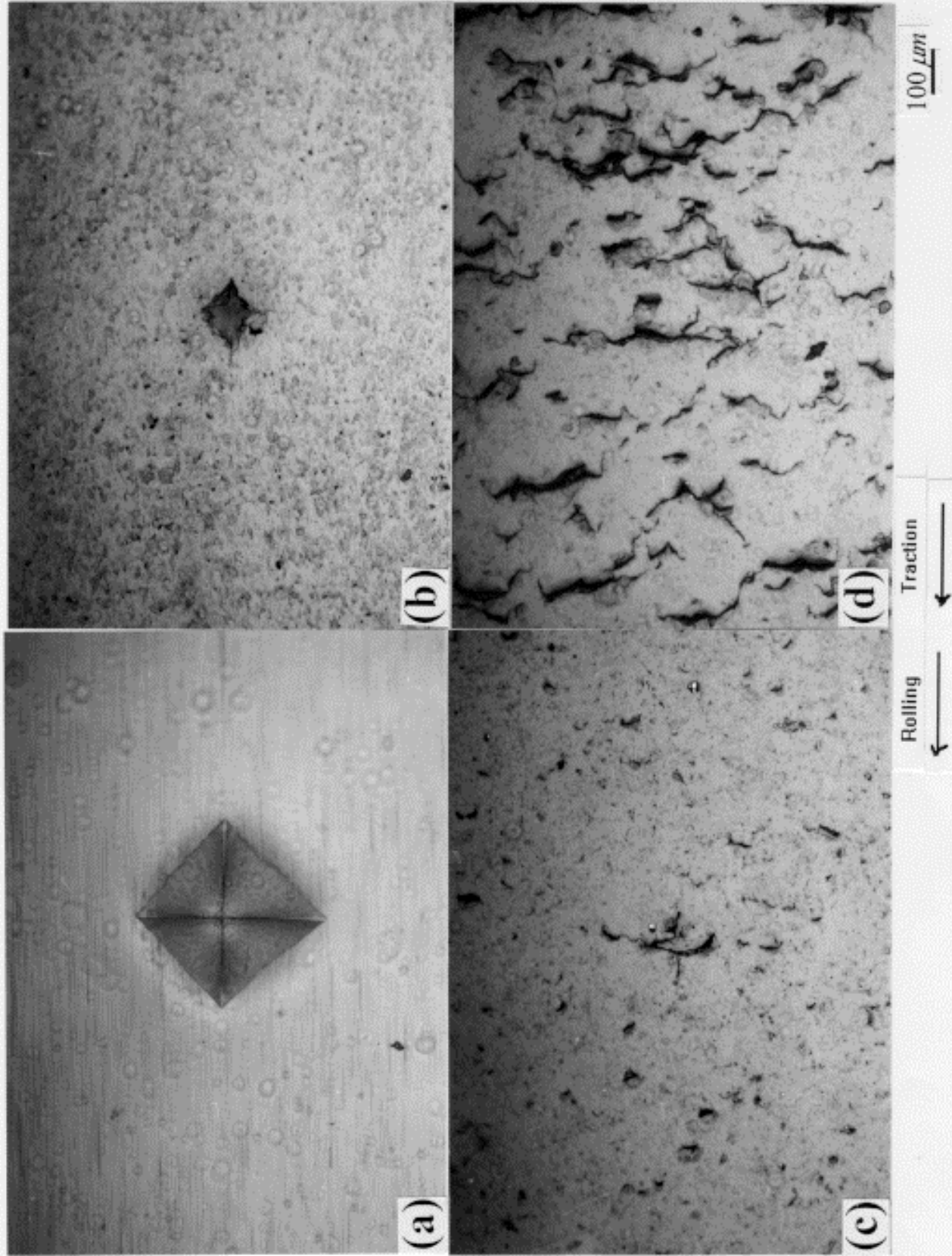
Figure 10. Progression of damage on the disc surface of rail around a pyramidal dent, $p_0 = 1500$ MPa, water lubrication. (a) $N = 0$; (b) $N = 5k$; (c) $N = 15k$; (d) $N = 40k$ cycles.
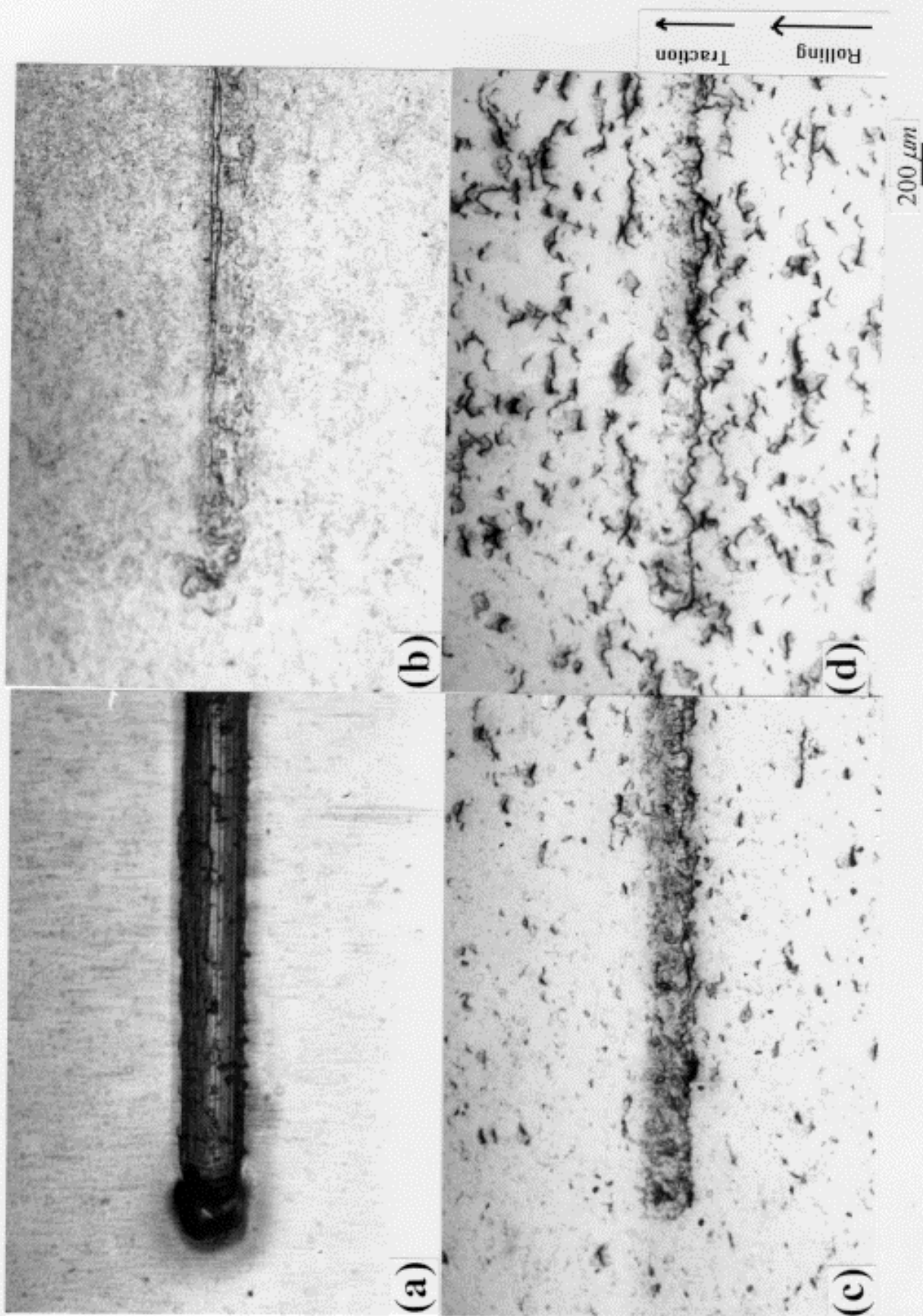
Figure 11. Morphology around a transverse furrow on the disc surface of rail, $p_0 = 1500$ MPa, water lubrication. (a) $N = 0$; (b) $N = 5k$; (c) $N = 20k$; (d) $N = 30k$ cycles.
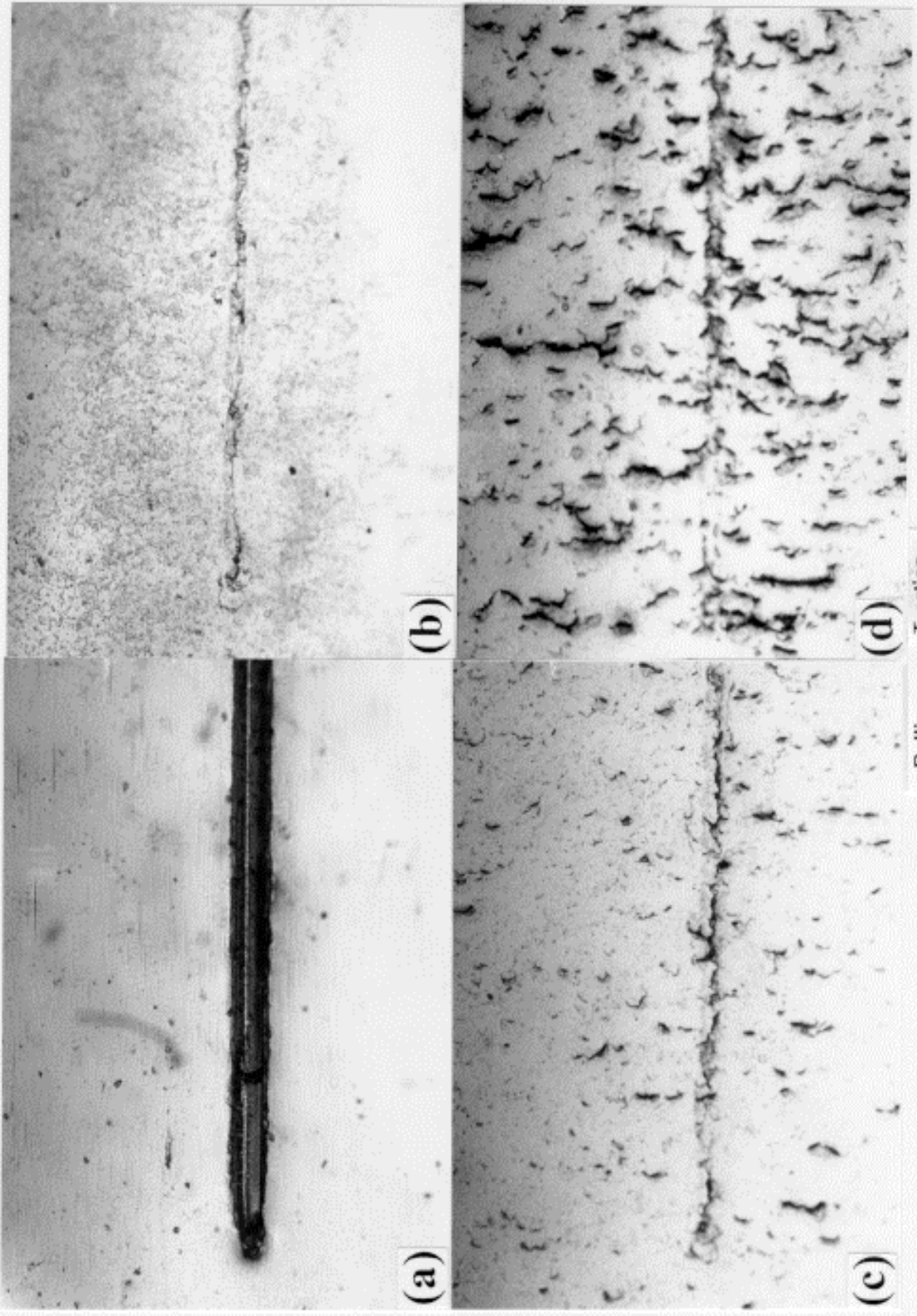
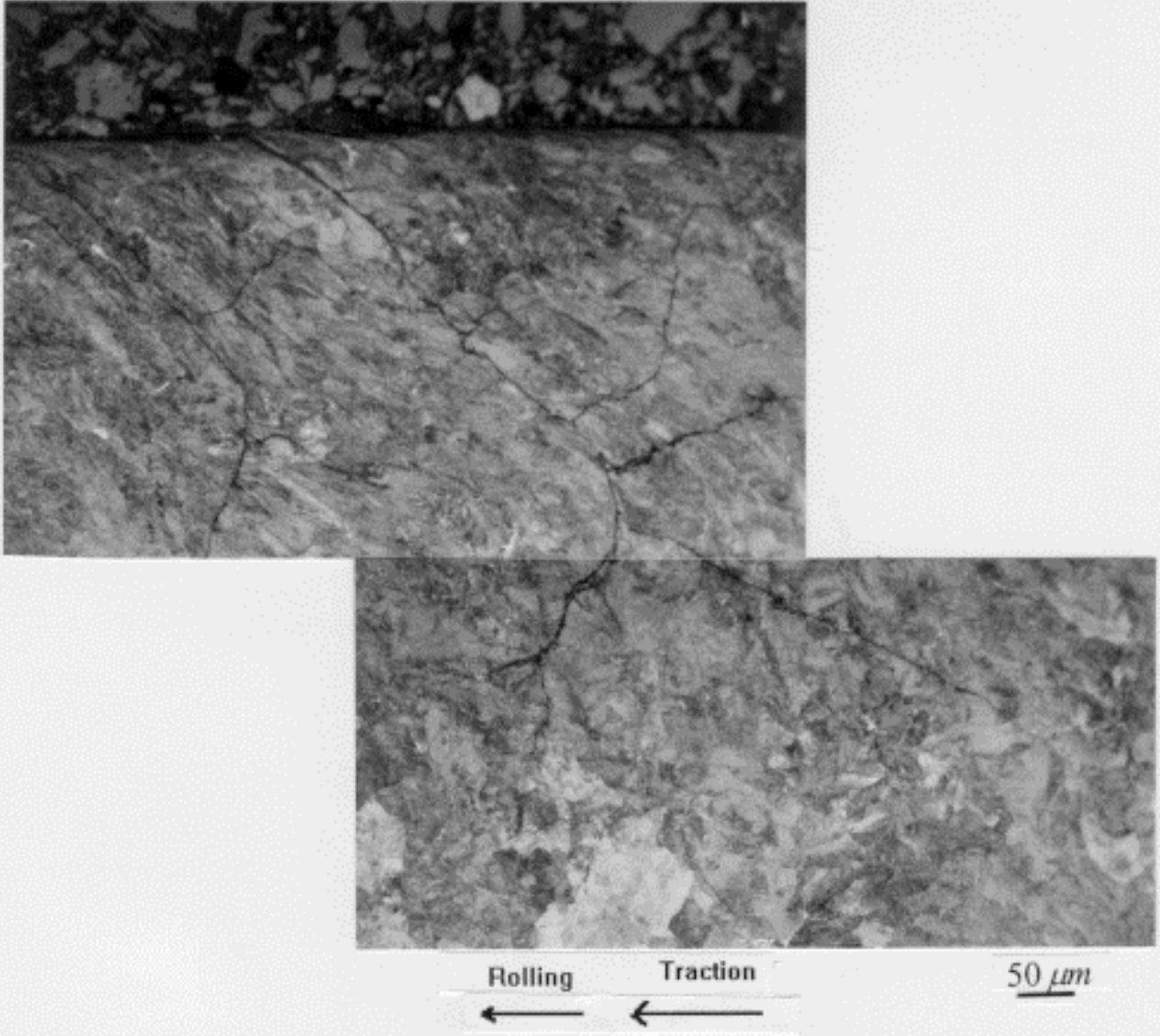Figure 12. Morphology around a longitudinal furrow on the disc surface of rail, p_0 = 1500 MPa, water lubrication.
(a) N = 0; (b) N = 5k; (c) N = 15k; (d) N = 30k cycles.

Figure 13. Morphology of crack growth observed from a sectioned rail surface, $p_0 = 1500$ MPa , water lubrication.
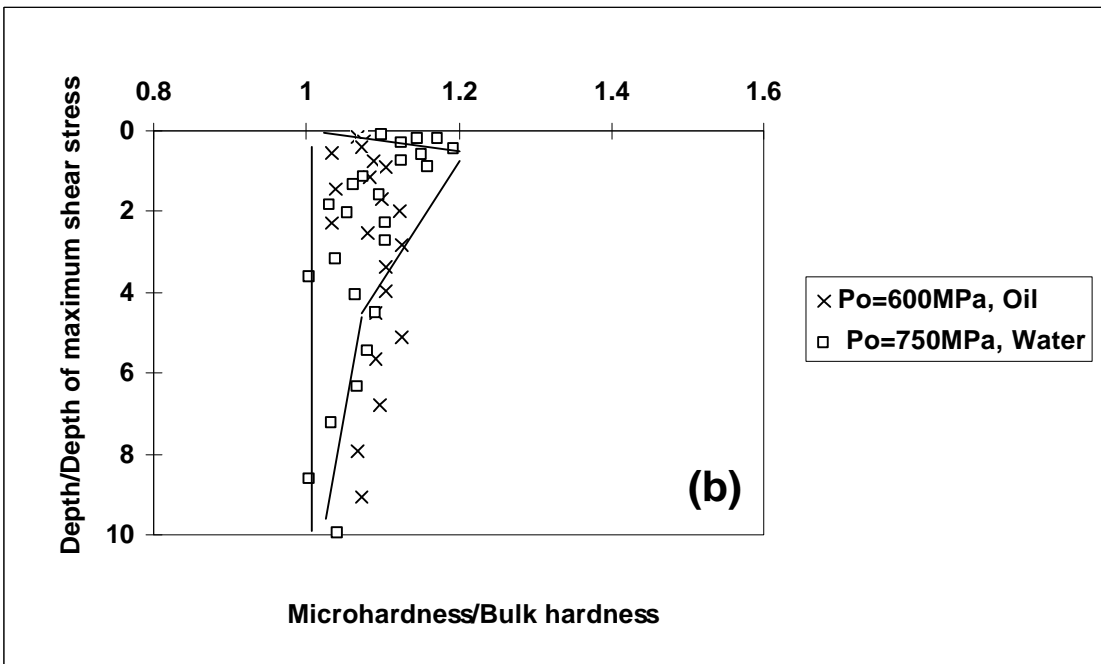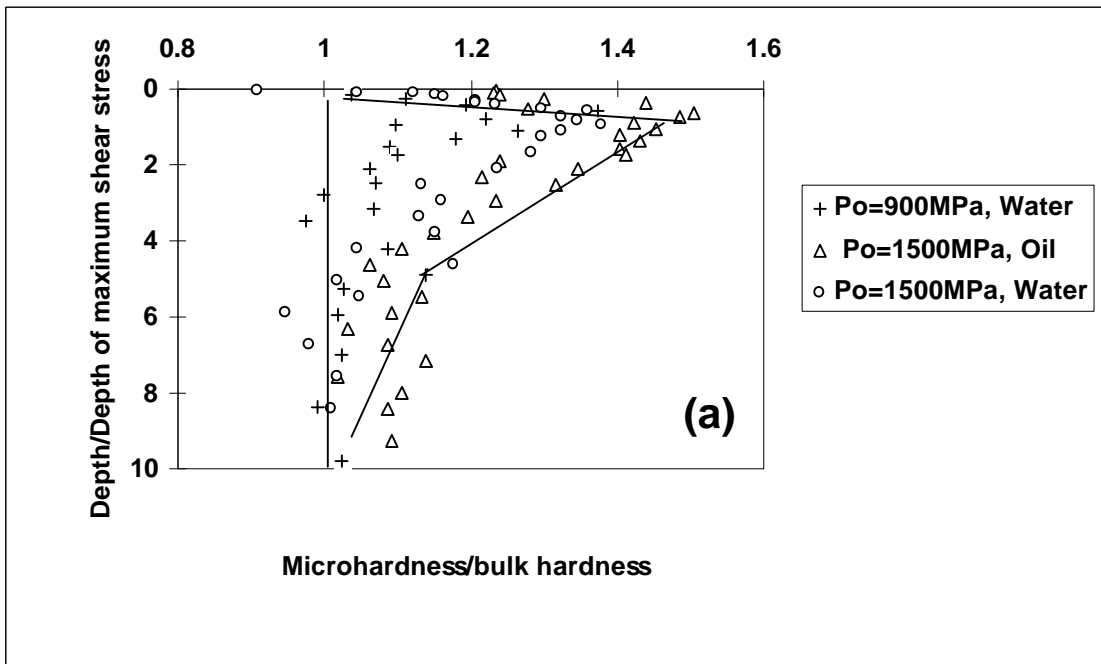
Figure 14. Hardness profile below the contact surface
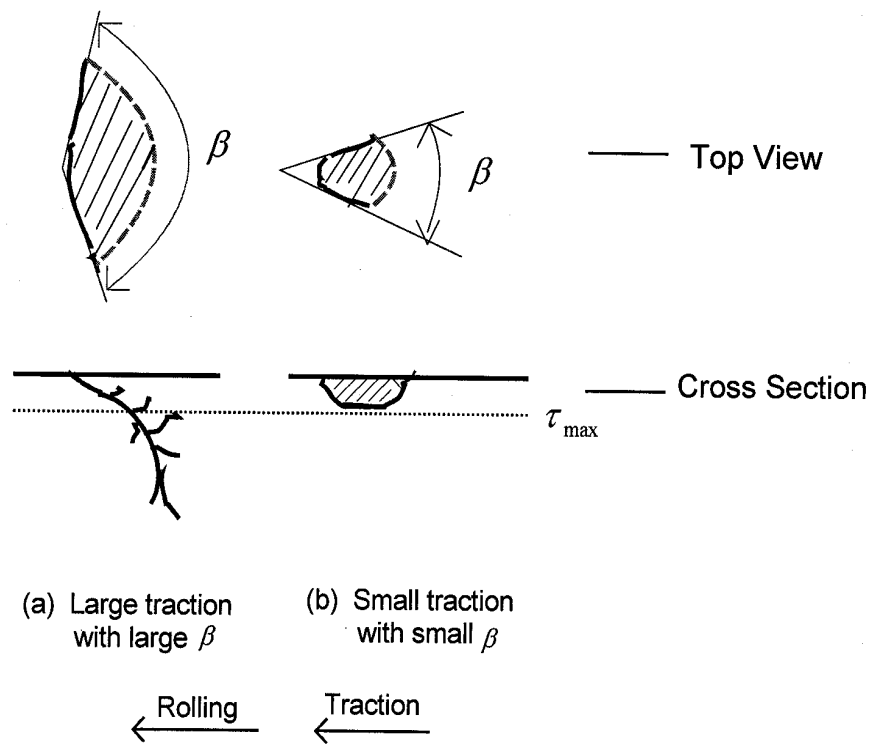under oil and water lubrication. (a) Rail; (b) Brass.

Figure 15 Schematic explanation of the effect of the friction on crack spread angle.